Balancing I/Q data in radar range-Doppler images

A. W. Doerry*

Sandia National Laboratories, P.O. Box 5800, MS 0519, Albuquerque, NM 87185

ABSTRACT

Modern high-performance radar systems' data is often rendered to distinguish between positive and negative frequencies necessitating complex data values, with real and imaginary constituents typically termed In-phase (I) and Quadrature (Q) elements respectively. Processing this data generally assumes well-balanced I/Q data, which may often be problematic due to non-ideal component and circuit behavior. We offer a number of techniques to mitigate the effects of I/Q imbalance.

Keywords: radar, balance, spurious, quadrature

1 INTRODUCTION

It has become the norm for modern high-performance radar systems to sample and digitize the raw radar returns for subsequent processing by Digital Signal Processing (DSP) techniques. Furthermore, the data is often rendered to distinguish between positive and negative frequencies necessitating complex data values, with real and imaginary constituents typically termed In-phase (I) and Quadrature (Q) elements respectively. Such techniques are common to

1. Synthetic Aperture Radar (SAR), and Inverse-SAR (ISAR),
2. Moving Target Indicator (MTI) radar, including Ground-MTI (GMTI) and similar radar modes, and
3. Wide-Area Search (WAS) modes, including Maritime-WAS (MWAS) and GMTI-WAS (GWAS) modes.

Signal path characteristics such as gain and phase to the point where I and Q signal elements become digital data requires a very high degree of balance in order to maintain signal integrity. Failure to do so will allow artifacts to be generated and degrade the radar's performance. Achieving an acceptable level of I/Q balance for some applications is problematic, requiring careful attention to system design and implementation. An oft-touted mitigation strategy is to collect digital data samples at an Intermediate Frequency (IF) and create I/Q components via Digital Signal Processing (DSP) techniques. Ostensibly, I/Q balance should then be perfect. But, as we shall show, this is somewhat optimistic.

Where it makes a difference, we shall herein presume a Linear-FM (LFM) chirp waveform with "stretch processing," as proposed by Caputi.[1] This is where the received echo analog signal is de-ramped, or de-chirped prior to digitization; a popular technique that allows wide-bandwidth echoes to be sampled at a lower data rate. This paper summarizes an earlier more comprehensive report on this topic.[2]

2 DISCUSSION – I/Q IMBALANCE

2.1 What Is It?

Consider a complex signal, with characteristics of variations in magnitude and phase, or equivalently with real and imaginary components. We identify this signal as

$$x(t) = A(t)\exp\left(jB(t)\right) = \alpha(t) + j\beta(t) \text{ = input signal (complex).} \quad (1)$$

* awdoerr@sandia.gov; phone 505-845-8165; www.sandia.gov/radar

where we identify the individual real-valued elemental function as

$A(t)$ = magnitude function,
$B(t)$ = phase function,
$\alpha(t)$ = real component of $x(t)$, and
$\beta(t)$ = imaginary component of $x(t)$. (2)

So, based on the Euler formula, the desired signal $x(t)$ can be written as

$$x(t) = A(t)\cos\big(B(t)\big) + jA(t)\sin\big(B(t)\big). \tag{3}$$

In fact, for real systems, due to the inescapable reality of non-ideal components, what are typically really created are perturbed components of the signal, both in amplitude and phase, or delay. That is, we really end up with signals more accurately described by

$$A(t)\cos\big(B(t)\big) \to \left(1+\frac{a}{2}\right)A\left(t-\frac{t_a}{2}\right)\cos\left(B\left(t-\frac{t_a}{2}\right)-\frac{\varphi_a}{2}\right), \text{ and}$$
$$A(t)\sin\big(B(t)\big) \to \left(1+\frac{a}{2}\right)^{-1}A\left(t+\frac{t_a}{2}\right)\sin\left(B\left(t+\frac{t_a}{2}\right)+\frac{\varphi_a}{2}\right), \tag{4}$$

Where a is the amplitude perturbation factor, t_a is the delay perturbation factor, and φ_a is the phase offset perturbation factor. When we think we are representing $x(t)$, we are actually representing a different signal

$$y(t) = \left\{\left(1+\frac{a}{2}\right)A\left(t-\frac{t_a}{2}\right)\cos\left(B\left(t-\frac{t_a}{2}\right)-\frac{\varphi_a}{2}\right)\right\} + j\left\{\left(1+\frac{a}{2}\right)^{-1}A\left(t+\frac{t_a}{2}\right)\sin\left(B\left(t+\frac{t_a}{2}\right)+\frac{\varphi_a}{2}\right)\right\}. \tag{5}$$

We note that the ratio of real to quadrature component amplitude is

$$\frac{\mathrm{Re}\{\max y(t)\}}{\mathrm{Im}\{\max y(t)\}} = \left(1+\frac{a}{2}\right)^2 \approx (1+a). \tag{6}$$

We also note that the phase difference between real and quadrature components is approximately

$$\angle\mathrm{Re}\{y(t)\} - \angle\mathrm{Im}\{y(t)\} = \left\{B\left(t-\frac{t_a}{2}\right) - B\left(t+\frac{t_a}{2}\right) - \varphi_a + \pi/2\right\} \approx \left\{-t_a\frac{d}{dt}B(t) - \varphi_a + \pi/2\right\}. \tag{7}$$

To be sure, for small perturbations, $y(t)$ looks very much like the desired signal $x(t)$, but it in fact is slightly different. Consequently, I/Q imbalance is perturbation of the relationship between Real and Imaginary components of the signal.

2.2 How Does It Manifest in the Range-Doppler Image?

We can assess the effects of the perturbation by decomposing the components of $y(t)$ as follows.

$$y(t) \approx y(t)\Big|_{\substack{a=0\\t_a=0\\\varphi_a=0}} + a\frac{\partial y(t)}{\partial a}\Big|_{\substack{a=0\\t_a=0\\\varphi_a=0}} + t_a\frac{\partial y(t)}{\partial t_a}\Big|_{\substack{a=0\\t_a=0\\\varphi_a=0}} + \varphi_a\frac{\partial y(t)}{\partial \varphi_a}\Big|_{\substack{a=0\\t_a=0\\\varphi_a=0}}. \tag{8}$$

Of course, this allows us to separate the original signal from the error manifestations, and by performing the partial derivatives, this can be expanded to

$$y(t) \approx x(t) + \left\{ \frac{aA(t) + j\varphi_a A(t) - t_a A'(t) + jt_a A(t)B'(t)}{2} \right\} \exp j\left(-B(t)\right), \tag{9}$$

where $A'(t)$ = time derivative of $A(t)$, and $B'(t)$ = time derivative of $B(t)$. This can be simplified to

$$y(t) \approx x(t) + \left[\frac{a + j\left(\varphi_a + t_a B'(t)\right)}{2} - \frac{t_a A'(t)}{2A(t)} \right] x^*(t) \tag{10}$$

where $x^*(t)$ is the complex conjugate of $x(t)$.

We observe the following

- Perturbations in amplitude, phase, and/or delay will cause the addition of an error signal that is the complex conjugate of the input signal.
- If the input signal is a complex sinusoid, then $A'(t) = 0$. In SAR images, point targets will exhibit $A'(t) = 0$.
- The error signal will exhibit opposite phase.
- The error signal will also exhibit opposite phase rate.
- In a range-Doppler image, this will manifest as both an opposite range offset, and an opposite Doppler offset. That is, this will manifest as a 'ghost' image reflected through the zero-range and zero-Doppler point, the actual DC point in the image.

We illustrate the effects of I/Q imbalance in Figure 1. The actual point targets are the brighter points in the bottom half of the image. For this example $a = 0.1$, resulting in I/Q imbalance ghosts at –26 dBc. In this case the DC point is at the center of the image. Note the ghost targets rotated 180 degrees about the central or DC point.

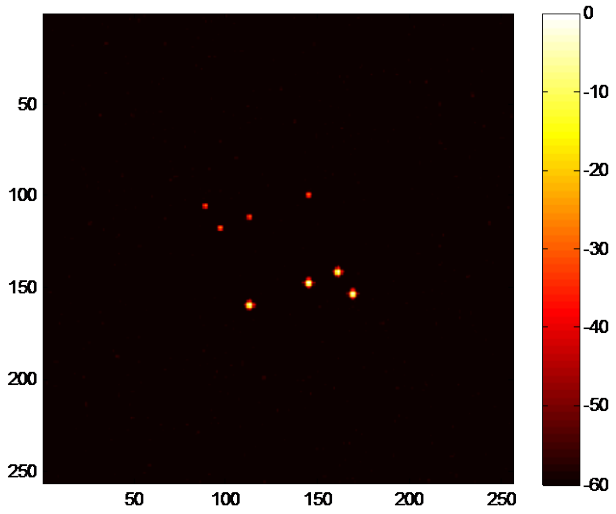

Figure 1. Example with I/Q Imbalance resulting in –26 dBc artifacts. The colorbar denotes dBc.

2.3 What Causes It?

We discuss below the typical root causes of I/Q imbalance.

2.3.1 Analog Down-Conversion to Quadrature Channels

We identify a real-valued IF signal as

$$x_{IF}(t) = x(t)e^{j2\pi f_{IF}t} + x^*(t)e^{-j2\pi f_{IF}t}. \tag{11}$$

where f_{IF} is the IF frequency on which the desired signal is modulated. We desire to extract or isolate the complex baseband signal $x(t)$. We accomplish this as follows. First we down-convert the IF signal to a baseband signal created and identified as

$$x_{baseband}(t) = x_{IF}(t)e^{-j2\pi f_{IF}t} = x(t) + x^*(t)e^{-j2\pi 2 f_{IF}t}. \tag{12}$$

Note that we may use the Euler formula and identify elemental signals

$$\begin{aligned} &\mathrm{Re}\{x_{baseband}(t)\} = x_{IF}(t)\cos(2\pi f_{IF}t), \text{ and} \\ &\mathrm{Im}\{x_{baseband}(t)\} = -x_{IF}(t)\sin(2\pi f_{IF}t). \end{aligned} \tag{13}$$

Analog lowpass filtering and subsequent sampling with Analog-to-Digital Converter (ADC) components of the down-converted signal yields

$$x_{ADC}(n) = x(n/f_s), \tag{14}$$

where f_s is the ADC sampling frequency, and the ADC samples are at uniformly spaced sample times of

$$t = n/f_s, \tag{15}$$

where n = sample index value. The architecture to accomplish this is illustrated in Figure 2. Note that we require two ADC components to implement this architecture. Clearly, if the two channels were not identical to each other in all but the IF demodulation employed, or the demodulation was not exactly $\pi/2$ radians apart in phase, then an imbalance would be generated in the ADC samples. Since we are talking about analog signal paths, imbalance to some degree is virtually guaranteed. Furthermore, balance levels required by modern high-performance radar systems are virtually impossible to achieve without further mitigation techniques.

2.3.2 Digital Down-Conversion to Quadrature Channels

We begin with a single ADC sampling the IF signal directly. It is particularly convenient for the input signal to be at an IF center frequency of $f_s/4$, that is, we will presume $f_{IF} = f_s/4$. Consequently, we identify the IF signal as

$$x_{IF}(t) = x(t)e^{j2\pi(f_s/4)t} + x^*(t)e^{-j2\pi(f_s/4)t}. \tag{16}$$

Recall that this signal is real-valued. Furthermore, $x(t)$ is band-limited to something less than $f_s/2$, and often to less than $f_s/4$. The ADC then generates the real-valued data samples described by

$$x_{ADC}(n) = x_{IF}(n/f_s). \tag{17}$$

The digital down-conversion (demodulation) is implemented as a complex multiplication with result

$$x_{dem}(n) = e^{-j(\pi/2)n}\left[x_{ADC}(n)\right] = x(n/f_s) + x^*(n/f_s)e^{-j\pi n}. \tag{18}$$

This normally undergoes additional low-pass filtering to remove the $e^{-j\pi n}$ modulated term, and typically some data decimation as well. We model the filtered demodulated signal as

$$x_{demfil}(n) = x(n/f_s)\ . \tag{19}$$

As stated, for digital down-conversion it is quite typical to build in some data decimation, usually by a factor of 4, so that the new data rate is in fact equal to the original IF frequency, which we recall as $f_{IF} = f_s/4$. However, for the purposes of this report we will ignore any decimation. It is this term that is of interest to us for further processing. Note that inadequate filtering may also ultimately cause unacceptable I/Q imbalance all by itself. We will ignore this, and assume that the filter was designed and operates correctly; in fact perfectly.

Consider the output of the digital down-conversion step $x_{dem}(n)$. We observe that the signal can be described with the following expansion.

$$x_{dem}(n) = (-j)^n\left[x_{ADC}(n)\right] = \begin{cases} x_{ADC}(n) & n = 0,4,8,... \\ -jx_{ADC}(n) & n = 1,5,9,... \\ -x_{ADC}(n) & n = 2,6,10,... \\ jx_{ADC}(n) & n = 3,7,11,... \end{cases}. \tag{20}$$

Note that even-valued values of index *n* yield purely real values for $x_{dem}(n)$, and odd-valued values for index *n* yield purely imaginary values for $x_{dem}(n)$. Combining some things, we identify explicitly the digital demodulation sequences as

$$\cos(2\pi f_{IF}t) = \cos\left(\frac{\pi}{2}n\right) = 1,0,-1,0,1,...\text{, and}$$
$$\sin(2\pi f_{IF}t) = \sin\left(\frac{\pi}{2}n\right) = 0,1,0,-1,0,... \tag{21}$$

The architecture to accomplish this is illustrated in Figure 3. Note that we require but a single ADC component to implement this architecture. The fact that this final demodulation can be accomplished by multiplications limited to 1, –1, and 0, is particularly attractive, and illustrates the utility of this digital down-conversion scheme, in particular the relationship of IF frequency to ADC sampling frequency.

2.3.2.1 Digital Down-Conversion with Clock Interference

Now consider that the ADC samples are taken at nonuniform-spaced sample times where the sample times are modulated at a rate of $f_s/2$. The model for these jittered sample times becomes

$$t = n/f_s - \cos\left(2\pi\left(\frac{f_s}{2}\right)(n/f_s)\right)(t_a/2) = n/f_s - (-1)^n(t_a/2). \tag{22}$$

The ADC samples then become the time-shifted (time-modulated) signal values

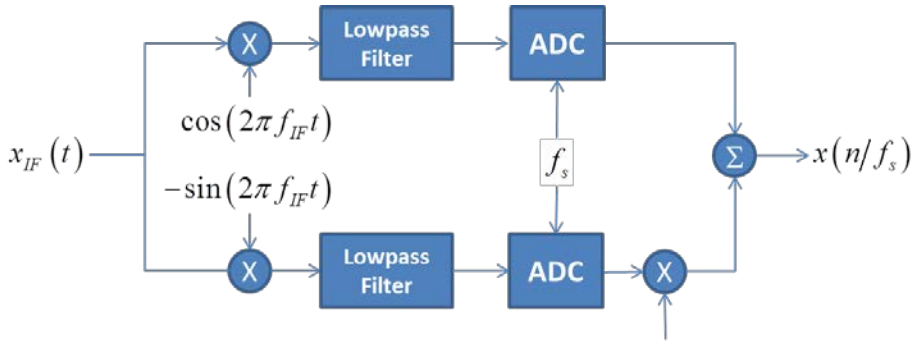

Figure 2. Analog down-conversion architecture.

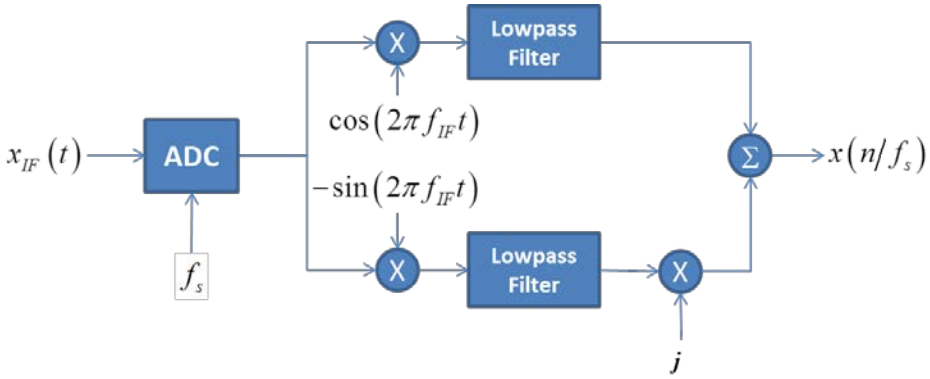

Figure 3. Digital down-conversion architecture. This is usually implemented with $f_{IF} = f_s/4$.

$$x_{ADC}(n) = x_{IF}\left(n/f_s - (-1)^n (t_a/2)\right). \tag{23}$$

Following the development given above, we observe that ultimately all real terms of $x_{dem}(n)$ are advanced by $(t_a/2)$, and all imaginary terms are retarded by $(t_a/2)$. Putting it all together yields

$$x_{demfil}(n) = \mathrm{Re}\left\{x\left(n/f_s - (t_a/2)\right)\right\} + j\,\mathrm{Im}\left\{x\left(n/f_s + (t_a/2)\right)\right\}. \tag{24}$$

Hence, ADC clock modulation resulting from some interference-source yields an I/Q imbalance. From the earlier analysis, we can describe the output signal as

$$x_{demfil}(n) \approx x(n/f_s) + \frac{t_a}{2}\left[jB'(n/f_s) - \frac{A'(n/f_s)}{A(n/f_s)}\right] x^*(n/f_s). \tag{25}$$

Point Target Response

Consider the case where the desired signal is described by the rotating phasor

$$x(t) = A_0 e^{j2\pi f_0 t}, \tag{26}$$

where A_0 is a constant amplitude, and f_0 is a constant frequency. This model is consistent with a point reflector radar echo after dechirping the echo response from an LFM chirp waveform. This allows the demodulated and filtered output samples to be described as

$$x_{demfil}(n) \approx x(n/f_s) + \frac{t_a}{2}\left[j2\pi f_0\right]x^*(n/f_s). \quad (27)$$

Interestingly, the amount of imbalance energy depends on the signal frequency f_0. In a range-Doppler image, this corresponds to the range offset of the target reflector.

2.3.2.2 Digital Down-Conversion with Ping-Pong ADCs

The foregoing analysis suggests that whenever digital down-conversion is used, any modulation applied to the ADC in any manner has the potential of manifesting an I/Q imbalance in the data. This is because of the feature that alternating raw ADC samples become I and Q data components respectively. In the previous section, we showed how Electromagnetic Interference (EMI) modulating the ADC strobe signal can cause I/Q imbalance. We put forward now that even in the absence of EMI, we may still have sample-to-sample modulation of the data.

Modern high-speed ADC components, of the sort that are normally attractive to radar designers, often achieve their high speed with an internal architecture that multiplexes two or more internal ADC functional blocks. In principle, this works great. However, also in principle, this relies on the application not being sensitive to subtle differences in the internal ADC functional blocks. In practice, we observe that

1. Real ADC functional blocks are not perfect, and exhibit some degree of nonlinearity.
2. Real ADC functional blocks are not identically imperfect. They exhibit different nonlinearities from each other.

The nonlinearity of an ADC conversion is often embodied in its Integrated Non-Linearity (INL) specification. There is also often a Differential Non-Linearity (DNL) specification as well. Nonlinearity affects gain. Different nonlinearities in ADC functional blocks affect gain differently in each functional block. Alternating between ADC functional blocks means alternating between signal gain characteristics. This in turn yields an amplitude modulation that is at a rate of $f_s/2$. This results in different gains for I values than for Q values, and hence an I/Q gain imbalance. Recall that an I/Q imbalance due to gain differences is not dependent on range offset in the image. However, it will be dependent on actual signal levels at the ADC.

2.3.2.3 Some Additional Comments

A detailed analysis of the internal operation of any particular ADC may reveal other possible EMI-based pathologies. While INL has been examined, we suggest that other EMI entry points into the ADC should not be neglected, such as the power and ground connections.

3 MITIGATION Techniques

Mitigation techniques for unwanted spurious energy are generally implemented with the following order of precedence.

1. Get rid of the spurious energy,
2. Move the spurious energy to unwanted signal space,
3. Smear the spurious energy to reduce its coherence and peak value, and
4. Reduce manifestation directly via image post-processing.

We examine these in turn. First, however, we note that mitigating the effects of I/Q imbalance is very related to mitigating the effects of other sources of spurious energy in a radar receiver, such as harmonic spurs due to ADC INL.[3]

3.1 Get Rid of It

For analog down-conversion architectures, where I and Q analog channels are created, if the imbalance is stable, then calibration might be employed to achieve improved balance. To achieve the required signal fidelity, the calibration might be for amplitude, phase, and/or delay, and furthermore may need to be a function of signal frequency. In practice, for some applications (like DMTI, etc.) it is quite difficult to achieve satisfactory performance.

In digital down-conversion architectures, I/Q imbalance in some cases can be a result of inadequate isolation of the susceptible ADC connections (e.g. clock, power, ground, etc.) from other inadvertent signal emitters. This is an EMI problem. Consequently, the preferred solution is EMI mitigation to effectively eliminate the coupling mechanism. This involves one or more of the following.

1. Reducing or eliminating EMI emissions at their source.
2. Decreasing the EMI coupling mechanism.
3. Reducing or eliminating the EMI susceptibility of the ADC clock and other ADC connections in the radar receiver. This is aided by good mixed-signal design practices as reported by Dudley.[4]

3.2 Move the Effects

In a typical SAR image, the scene of interest is only a portion of the overall Doppler bandwidth, and sometimes a very small portion. Consequently, if the imbalance energy can be moved to a Doppler region that will be cropped away, then it will not appear in the image. A technique for doing this is presented in a patent by Doerry and Tise.[5] We briefly repeat a description of this technique here. Recall that the IF input signal is given by Eq. (11). Now let us create a new IF signal that incorporates a particular pulse-dependent rolling phase shift and is described as

$$x_{IF,ps}(t,m) = x(t)e^{j2\pi f_{IF}t}\, e^{j2\pi(1/4)m} + x^*(t)e^{-j2\pi f_{IF}t}e^{-j2\pi(1/4)m}, \tag{28}$$

where m is the pulse index number. Note that $e^{j2\pi(1/4)m}$ represents a $\pi/4$ phase accumulation with each increment in pulse index. If this is the signal that is sampled, and then undergoes digital down-conversion, then the demodulated and filtered signal may be expanded to

$$x_{demfil,ps}(n,m) \approx x(n/f_s)e^{j2\pi(1/4)m} + C_{imbalance}\, x^*(n/f_s)e^{-j2\pi(1/4)m}, \tag{29}$$

where $C_{imbalance}$ represents the scaling that results of the imbalance energy. Finally, we remove the previously inserted pulse-dependent phase shift by multiplying the digital data with the opposite pulse-dependent phase shift of $e^{-j2\pi(1/4)m}$, which yields

$$x_{demfil}(n,m) = x(n/f_s) + C_{imbalance}\, x^*(n/f_s)e^{-j\pi m}. \tag{30}$$

We note the following.

- The output contains the signal $x(n/f_s)$ as desired. This is good.
- The conjugate term $x^*(n/f_s)$ is modulated by $e^{-j\pi m}$, which shifts the ghost echoes by half the image extent in azimuth (Doppler).
- It is important that the rolling phase shift be applied before the I/Q imbalance occurs, and then removed afterwards. That is, for digital down-conversion, this is normally applied before the ADC, and removed from the data after the ADC.

- For a range-Doppler image, e.g. SAR, a tacit requirement is that the radar PRF be at least twice the Doppler bandwidth of the in-beam clutter. That is the 'shifted to' region has to be at least as large as the 'shifted from' region in Doppler. The 'shifted to' region is then cropped away, thereby removing the I/Q imbalance energy.
- For GMTI and other techniques that use the larger Doppler space, including the exo-clutter region, this technique is not appropriate. That is, generally the 'shifted to' region is not cropped away.

This effect of this technique is illustrated in Figure 4, with shifted imbalance artifacts. We further note that this is effectively a commutation technique.[6]

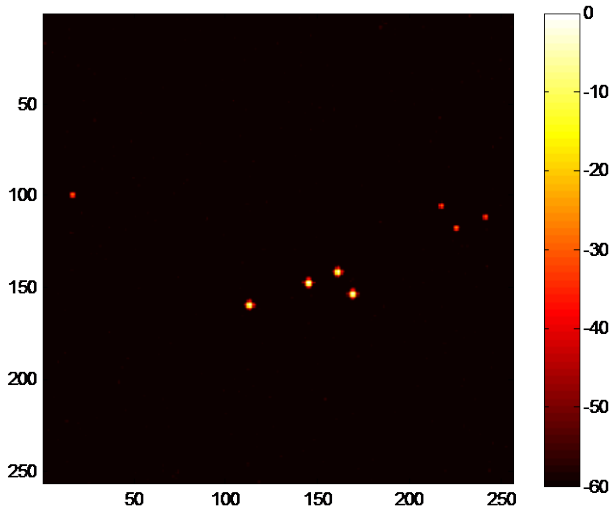

Figure 4. Example of Figure 1 but with rolling phase shift prior to ADC. For convenience, we have allowed the imbalance to be constant for all targets. Note that the anomalous responses have been shifted to the edge of the image, but the true signals are properly located.

3.3 Smear the Effects

If the offending I/Q imbalance energy cannot be suppressed or moved to a harmless location in the range-Doppler space, then the next best mitigation strategy normally is to smear the imbalance energy by reducing its coherence, thereby reducing its obviousness in the range-Doppler map. This is simply diluting the imbalance energy. The smearing can be applied in either or both of the range and Doppler directions.

3.3.1 Range Smearing

A convenient means of smearing the I/Q imbalance energy in range is to impart a quadratic phase error in range to the imbalance energy. The effect of a quadratic phase error on impulse response is discussed in an earlier report by Doerry.[7] Of course, since a quadratic phase error is simply a LFM chirp, one way to impart a quadratic phase error onto the imbalance energy is to leave a residual chirp on the data after the normal de-chirping operation. This is discussed in a patent by Dubbert & Tise.[8] Here we briefly discuss the details of why a residual chirp helps with smearing I/Q imbalance energy. Recall that the IF input signal is given by Eq. (11). Now let us create a new IF signal that incorporates a residual chirp, due to perhaps not completely de-chirping the radar echo energy. We describe this residual chirp effect as

$$x_{IF,rc}(t) = x(t)e^{j2\pi f_{IF}t}e^{j2\pi(\gamma_{rc}/2)t^2} + x^*(t)e^{-j2\pi f_{IF}t}e^{-j2\pi(\gamma_{rc}/2)t^2}, \tag{31}$$

where γ_{rc} = residual chirp rate. We now define an equivalent input signal with the phase shift as

$$x_{rc}(t) = x(t)e^{j2\pi(\gamma_{rc}/2)t^2} . \tag{32}$$

By sampling at IF, demodulating, and filtering the signal, we may identify the sampled result as

$$x_{demfil,rc}(n) \approx \left[x(n/f_s)e^{j2\pi(\gamma_{rc}/2)(n/f_s)^2} + C_{imbalance}\, x^*(n/f_s)e^{-j2\pi(\gamma_{rc}/2)(n/f_s)^2} \right]. \tag{33}$$

Finally, we remove the previously inserted time-dependent phase shift, and simplify to

$$x_{demfil}(n) = e^{-j2\pi(\gamma_{rc}/2)(n/f_s)^2} x_{demfil,rc}(n) = x(n/f_s) + C_{imbalance}\, x^*(n/f_s)e^{-j2\pi(\gamma_{rc})(n/f_s)^2} . \tag{34}$$

We note the following.

- The output contains the signal $x(n/f_s)$ as desired. This is good.
- The conjugate term $x^*(n/f_s)$ is modulated by $e^{-j2\pi(\gamma_{rc})(n/f_s)^2}$, which is a residual chirp at twice the chirp rate of the original residual chirp prior to the ADC. Consequently, the imbalance energy is smeared.
- It is important that the residual chirp be applied before the I/Q imbalance occurs, and then removed afterwards. That is, for digital down-conversion, this is normally applied before the ADC, and removed from the data after the ADC.

The relevant parameter of the residual chirp is its time-bandwidth product. The time-bandwidth product of the imbalance energy in the final image is twice the original time-bandwidth product, and is also the amount of smearing as measured at the –3 dB points of the smeared response in terms of resolution units.

This effect of this technique is illustrated in Figure 5. In this example, the sampled data retained a residual chirp with a time-bandwidth product of 10. This means that the I/Q imbalance of Figure 1 is smeared in the final image with a residual chirp with time-bandwidth product of 20. Theoretically this should reduce peak value of the imbalance energy by approximately 12 dB, accounting for the smearing not being entirely 'flat'. In this example, we in fact measured a peak value for I/Q imbalance of –38 dBc, for a reduction of 12 dB.

3.3.2 Azimuth Smearing

As with the residual chirp for range smearing, accomplishing smearing in azimuth requires applying and removing a phase modulation in the raw data in azimuth, that is, on a pulse-to-pulse basis. We examine this here. Recall once again that the IF input signal is given by Eq. (11). Now let us create a new IF signal that incorporates a particular pulse-dependent generalized phase shift and is described as

$$x_{IF,rp}(t,m) = x(t)e^{j2\pi f_{IF}t}\, e^{j\varphi(m)} + x^*(t)e^{-j2\pi f_{IF}t}e^{-j\varphi(m)}, \tag{35}$$

where $\varphi(m)$ is a generalized pulse-dependent phase value. The nature of $\varphi(m)$ may be a specific function, or perhaps selections from a set of random values. For smearing, we will require $\varphi(m)$ to be nonlinear with *m*. We now define an equivalent input signal with the phase shift as

$$x_{rp}(t,m) = x(t)e^{j\varphi(m)} . \tag{36}$$

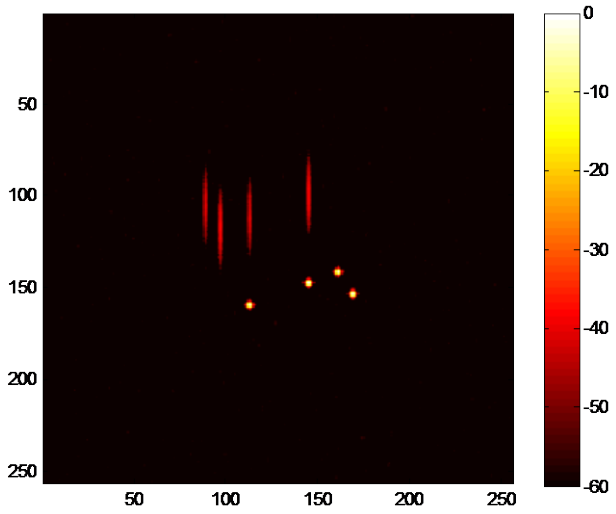

Figure 5. Example of Figure 1 but with a residual chirp applied prior to ADC. For convenience, we have allowed the imbalance to be constant for all targets. Note that the anomalous responses have been smeared in range and reduced in peak value by a measured 12 dB.

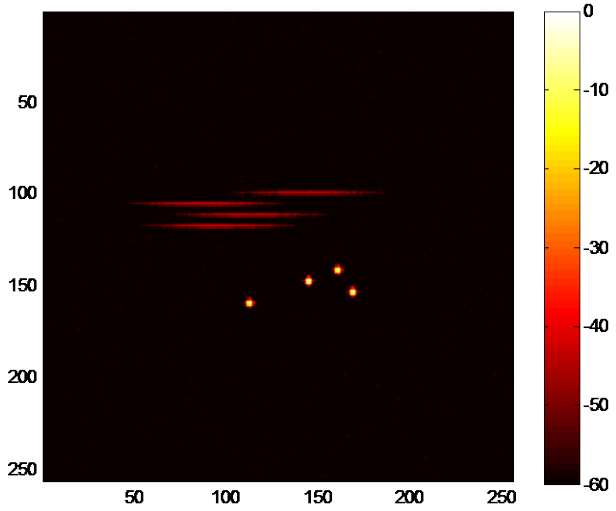

Figure 6. Example of Figure 1 but with quadratic pulse-dependent phase shift prior to ADC. For convenience, we have allowed the imbalance to be constant for all targets. Note that the anomalous responses have been smeared substantially in azimuth, but the true signals are properly located.

By sampling at IF, demodulating, and filtering the signal, we may identify the sampled result as

$$x_{demfil,rp}(n,m) \approx x(n/f_s)e^{j\varphi(m)} + C_{imbalance}\,x^*(n/f_s)e^{-j\varphi(m)}. \tag{37}$$

Finally, we remove the previously inserted sample-dependent phase shift, and simplify to

$$x_{demfil}(n,m) = e^{-j\varphi(m)} x_{demfil,rp}(n,m) = x(n/f_s) + C_{imbalance}\, x^*(n/f_s) e^{-j2\varphi(m)}. \quad (38)$$

We note the following.

- The output contains the signal $x(n/f_s)$ as desired. This is good.
- The conjugate term $x^*(n/f_s)$ is modulated by $e^{-j2\varphi(m)}$, which is twice the phase as what was applied.
- With proper modulation of phase shifts, the imbalance energy will smear in azimuth, perhaps even across the entire Doppler space. A proper phase shift modulation is one for which $e^{-j2\varphi(m)}$ will still cause smearing, that is, for example, does not degenerate to a constant. This is addressed more completely below.
- It is important that the phase shift be applied before the I/Q imbalance occurs, and then removed afterwards. That is, for digital down-conversion, this is normally applied before the ADC, and removed from the data after the ADC.

3.3.2.1 Azimuth Chirps

As with the residual chirp technique, we can spread imbalance energy in azimuth by applying an azimuth chirp prior to the ADC and removing it afterwards. This is implemented via a quadratic phase modulation.

The effect of quadratic phase modulation is illustrated in Figure 6. In this example, a quadratic phase function with time-bandwidth product of 20 was applied and then removed from the data. The smearing across the Doppler space for this example should theoretically reduce the peak imbalance energy by approximately 15 dB. In this example, we in fact measured a peak value for I/Q imbalance of –41 dBc, for a reduction of 15 dB. Larger time-bandwidth products would improve this, although at some point aliasing would cause constructive interference leading to peak imbalance energy levels even larger yet than theoretical.

3.3.2.2 Pulse Random Phase Coding

We now address a random phase error of some type applied on a pulse to pulse basis. Any random phase modulation applied will be 'doubled' in phase value, which except in pathological cases retains its randomness. Consequently, the imbalance energy is affected by a random phase modulation. The Doppler processing implements a filter bank. However, filtering a random signal yields only another random signal. Uncorrelated phase modulation will yield a 'white' spectrum in the image. Central Limit Theorem arguments indicate that in the final image, the phase modulation will yield White Gaussian Noise, manifested as a streak across the Doppler spectrum with complex Gaussian characteristics. The magnitude would of course be Rayleigh distributed.

Essentially, the random phase modulation will smear the imbalance energy into a noisy streak across the Doppler space. The noisy streak will have magnitude peaks substantially higher than the magnitude average, consistent with the Rayleigh distribution. Statistically, a uniform smearing across Doppler will yield a reduction in imbalance energy approximately equal to the number of pulses. However, this is for a uniform distribution of energy across the Doppler spectrum. The random nature of the noisy streak will cause individual pixels to depart from this, and allow substantially higher peak values. The peak value is again a statistical value, based on the Rayleigh distribution. Typical peak to mean values encountered are in the range of 8-10 dB. Greater values are more likely encountered with larger Doppler dimensions, due to more opportunities.

The effect of random phase modulation is illustrated in Figure 7. In this example, random values from a continuum of values in the range $[0,2\pi)$ were applied and then removed from the data. A uniform smearing across the Doppler space for this example would theoretically reduce the peak imbalance energy by 23 dB (assuming the –35 dB Taylor window with nbar = 4). Allowing for an 8 dB peak to average discount, we would expect perhaps a 15 dB reduction in peak I/Q imbalance energy. In this example, we in fact measured a peak value for I/Q imbalance of –41 dBc, for a reduction of 15 dB. We do note in the image that the smearing is not absolutely uniform, as expected.

3.3.2.3 Pulse Quantized Random Phase Coding

We state here without elaboration that if the random phases are quantized to some set of phases, we must remain mindful that the residual phase in the demodulated data is twice the initially applied phase. This is particularly problematic when the applied random phase is limited of values of 0 and π radians.

3.3.3 Combined Range and Azimuth Smearing

In previous sections we analyzed range smearing via a residual chirp, and azimuth smearing via quadratic and random phase coding. We observe that we may combine range and azimuth smearing, and simultaneously do both. All the previously developed constraints still apply.

3.4 Image Post-Processing

Here we concern ourselves with operations after the range-Doppler image has been formed, and still contains manifestations of I/Q imbalance in the original data.

3.4.1 Image Ghost Subtraction

The locations of I/Q imbalance artifacts are deterministic. That is, we know that the energy is symmetrical across the DC point in the range-Doppler image. This suggests that the imbalance energy might be subtracted from the image by subtracting a rotated and scaled version of the original image from the original image itself. We note, however, that care must be taken to rotate the subtracted image in the range-Doppler space of the image, or otherwise account for any range-Doppler warping to effect geometric corrections due to wavefront curvature. We also note that this subtraction technique works best if no other I/Q imbalance mitigation techniques are employed, say, to smear the I/Q imbalance energy.

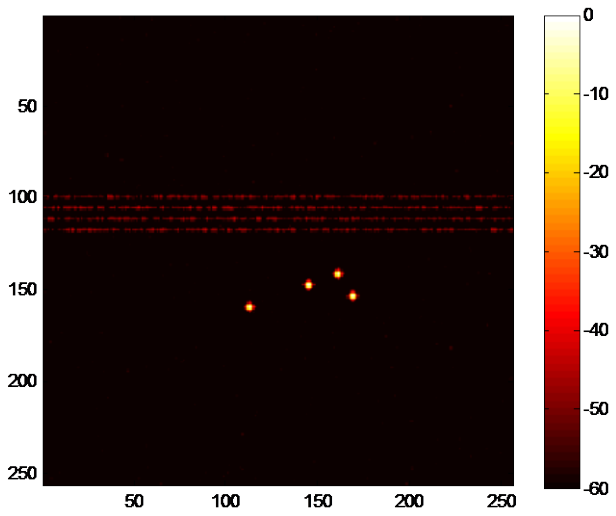

Figure 7. Example of Figure 1 but with pulse-dependent random phase shift prior to ADC. For convenience, we have allowed the imbalance to be constant for all targets. Note that the anomalous responses have been smeared across the extent of the image, but the true signals are properly located.

3.4.2 I/Q Imbalance Spur Apodization

A recent report by Doerry and Bickel[9] presents a technique for cropping or apodizing spurious energy due to I/Q imbalance among other sources. This technique passes the signal through two parallel channels, each with different pulse-to-pulse phase modulations applied, and then compares the two resulting range-Doppler images. As previously

shown, I/Q imbalance spurs are displaced by such modulations. Any energy not common to both channels, i.e. collocated in both images, is deemed a spurious response and discarded or otherwise attenuated in some fashion.

4 SUMMARY & CONCLUSIONS

We offer several summary comments.

- It is difficult to match real components in analog down-conversion techniques such that the I and Q channels are sufficiently balanced.
- In spite of IF sampling and digital down-conversion, I/Q imbalance can still manifest in the sampled data.
- EMI can cause I/Q imbalance.
- ADC ping-pong operation can also cause I/Q imbalance, due to INL differences.
- Pulse-to-pulse phase modulation can move the imbalance energy to otherwise cropped Doppler space for some range-Doppler (e.g. SAR) images. This is not viable for GMTI.
- Combinations of residual chirps in range, and pulse to pulse phase modulation can substantially smear the imbalance energy by several tens of dB.
- When all else fails, it is sometimes possible to use image processing to substantially diminish the manifestation of I/Q imbalance in the range-Doppler images themselves.

ACKNOWLEDGEMENTS

Sandia National Laboratories is a multi-program laboratory managed and operated by Sandia Corporation, a wholly owned subsidiary of Lockheed Martin Corporation, for the U.S. Department of Energy's National Nuclear Security Administration under contract DE-AC04-94AL85000.

REFERENCES

[1] William J. Caputi, Jr., "Stretch: A Time-Transformation Technique," *IEEE Transactions on Aerospace and Electronic Systems*, Vol. AES-7, No. 2, pp 269-278, March 1971.

[2] Armin W. Doerry, "Mitigating I/Q Imbalance in Range-Doppler Images," Sandia Report SAND2014-2252, Unlimited Release, March 2014.

[3] Armin W. Doerry, Dale F. Dubbert, Bert L. Tise, "Effects of Analog-to-Digital Converter Nonlinearities on Radar Range-Doppler Maps," Sandia Report SAND2014-15909, Unlimited Release, July 2014.

[4] Peter Dudley, "Design Guidelines for SAR Digital Receiver/Exciter Boards", Sandia Report SAND2009-7276, Unlimited Release, November 2009.

[5] Armin W. Doerry, Bertice L. Tise, "Correction of I/Q channel errors without calibration," US Patent 6,469,661, October 22, 2002.

[6] Armin W. Doerry, "Radar Channel Balancing with Commutation," Sandia Report SAND2014-1071, Unlimited Release, February 2014.

[7] Armin W. Doerry, "SAR Impulse Response with Residual Chirps", Sandia Report SAND2009-2957, Unlimited Release, June 2009.

[8] Dale Dubbert, Bert Tise, "Radar echo processing with partitioned de-ramp," US Patent 8,400,349, March 19, 2013.

[9] Armin W. Doerry, Douglas L. Bickel, "Apodization of Spurs in Radar Receivers Using Multi-Channel Processing," Sandia Report SAND2014-1678, Unlimited Release, March 2014.